AGU PUBLICATIONS

JGR

Journal of Geophysical Research: Space Physics

RESEARCH ARTICLE
10.1002/2015JA020999

Pathways of *F* region thermospheric mass density enhancement via soft electron precipitation

B. Zhang[1], R. H. Varney[2], W. Lotko[1], O. J. Brambles[1], W. Wang[2], J. Lei[3], M. Wiltberger[2], and J. G. Lyon[4]

[1]Thayer School of Engineering, Dartmouth College, Hanover, New Hampshire, USA, [2]High-Altitude Observatory, National Center for Atmospheric Research, Boulder, Colorado, USA, [3]School of Earth and Space Sciences, University of Science and Technology of China, Hefei, China, [4]Department of Physics and Astronomy, Dartmouth College, Hanover, New Hampshire, USA

Key Points:
- Soft electrons affect *F* region thermospheric mass density
- The indirect heating pathway is efficient during active periods
- The direct heating pathway is relatively inefficient

Correspondence to:
B. Zhang,
bzhang@dartmouth.edu

Citation:
Zhang, B., R. H. Varney, W. Lotko, O. J. Brambles, W. Wang, J. Lei, M. Wiltberger, and J. G. Lyon (2015), Pathways of *F* region thermospheric mass density enhancement via soft electron precipitation, *J. Geophys. Res. Space Physics*, *120*, 5824–5831, doi:10.1002/2015JA020999.

Received 12 JAN 2015
Accepted 29 MAY 2015
Accepted article online 2 JUN 2015
Published online 14 JUL 2015

Abstract The efficiencies of pathways of thermospheric heating via soft electron precipitation in the dayside cusp region are investigated using the coupled magnetosphere-ionosphere-thermosphere model (CMIT). Event-based data-model comparisons show that the CMIT model is capable of reproducing the thermospheric mass density variations measured by the CHAMP satellite during both quite and active periods. During the 24 August 2005 storm event ($Kp = 6-$) while intense Joule heating rate occurs in the polar cusp region, including soft electron precipitation is important for accurately modeling the *F* region thermospheric mass density distribution near the cusp region. During the 27 July 2007 event ($Kp = 2-$) while little Joule heating rate occurs in the polar cusp region, the controlled CMIT simulations suggest that the direct pathway through the energy exchange between soft electrons and thermospheric neutrals is the dominant process during this event, which only has a small effect on the neutral temperature and mass density at 400 km altitude. Comparisons between the two case studies show that the indirect pathway via increasing the *F* region Joule heating rate is a dominant process during the 24 August 2005 storm event, which is much more efficient than the direct heating process.

1. Introduction

Accurate prediction of Earth's thermospheric mass density is important from the perspectives of both space weather prediction and space science research. For example, knowledge of the distribution and evolution of thermospheric mass density is crucial for tracking low-Earth-orbiting satellites since the drag on a satellite is regulated by the total mass density of the thermosphere. In the dayside cusp region near 400 km altitude, significant thermospheric mass density enhancements on the order of 20%–200% above the background density have been observed by the CHAMP and Gravity Recovery and Climate Experiment satellites during both geomagnetic quite and active periods. The global distributions of thermospheric mass density derived from CHAMP accelerometer measurements also exhibit larger density in the cusp and premidnight auroral zone up to 30% relative to the Mass Spectrometer Incoherent Scatter (MSIS90) empirical model [*Liu et al.*, 2005].

Several physical processes have been considered to be drivers for the observed *F* region thermospheric mass density enhancement in the cusp region. The first driver is the Joule heating in the cusp region associated with an enhancement in the convection electric field [e.g., *Demars and Schunk*, 2007; *Crowley et al.*, 2010; *Knipp et al.*, 2011; *Carlson et al.*, 2012]. The enhanced Joule heating causes an increase of neutral temperature through ion-neutral frictional heating which leads to upwelling of thermospheric neutrals. A statistical study showed that merging electric field may be a suitable driver for the relative enhancement of the dayside thermospheric mass density during nonstorm times [*Rentz and Lühr*, 2008]. *Crowley et al.* [2010] found that during a strong interplanetary magnetic field (IMF) B_y driving event while the activity indices were low, when using the Joule heating pattern derived from the assimilative mapping of ionospheric electrodynamics model [*Richmond*, 1992], the enhancement of thermospheric density can be qualitatively reproduced by the thermosphere-ionosphere-mesosphere electrodynamics general circulation model (TIMEGCM) [*Roble and Ridley*, 1994]. However, this study could not produce quantitative agreement on the relative enhancement of thermospheric mass density with observations. *Crowley et al.* [2010] showed that when only Joule heating is considered in TIMEGCM, the thermospheric mass density in the cusp region at CHAMP altitude is enhanced

by approximately 30% relative to the background mass density, which is smaller than the observed value of approximately 200%. *Liu et al.* [2010] also showed that during storm time, Joule heating may also be a driver for the upwelling of thermospheric mass density. The second driver is soft electron precipitation in the dayside cusp region [e.g., *Rentz*, 2009; *Zhang et al.*, 2012; *Deng et al.*, 2013]. The thermospheric heating via soft electron precipitation has two pathways. The direct pathway is defined as the heating associated with direct energy exchange between precipitating soft electrons and *F* region ions/neutrals. The indirect pathway is through influencing the *F* region ionization and conductivity above 150 km, which affects the altitudinal distribution of Joule heating rate. Theoretical studies suggest that soft electrons may affect the thermospheric mass density more efficiently through the indirect pathway, that is, via increasing the Joule heating rate in the *F* region, in which the heating is more efficient than that in the *E* region [*Deng et al.*, 2011; *Huang et al.*, 2012]. Similar conclusions regarding the relative efficiencies of the direct and indirect heating pathways were also found using idealized, non-self-consistent controlled simulations from the Global Ionosphere Thermosphere Model [*Deng et al.*, 2013]. A third driver results from small-scale processes such as localized heating associated with field-aligned current (FAC) filaments (1 km size). *Lühr* [2004] used CHAMP observations to show correlations between *F* region mass density enhancements and the appearance of intense FACs with amplitudes of several hundreds of mA/m^2. For northward IMF driving conditions, about a half of the observed density enhancements are accompanied by strong FAC filaments [*Liu et al.*, 2010]. Another possible candidate for thermospheric heating is ion-neutral friction in the F_2 layer within subauroral polarization streams [*Wang et al.*, 2011; *Mishin et al.*, 2012].

In this paper, we investigate the direct and indirect roles of cusp soft electron precipitation on the enhancement of *F* region thermospheric neutral density. The physical processes associated with soft electron precipitation as a driver for thermospheric mass density enhancement in the dayside cusp region are investigated based on two event-based simulations using the self-consistent, coupled magnetosphere-ionosphere-thermosphere (CMIT) model [*Wiltberger et al.*, 2004; *Wang et al.*, 2004]. Data derived from the CHAMP satellite are used to validate the simulation results. The CMIT model combines the Lyon-Fedder-Mobarry (LFM) global magnetosphere simulation [*Lyon et al.*, 2004; *Merkin and Lyon*, 2010] and the thermosphere-ionosphere-electrodynamics general circulation model (TIEGCM) [*Roble et al.*, 1988] through the Magnetosphere Ionosphere Coupler/Solver model [*Merkin and Lyon*, 2010]. In the CMIT model, LFM is driven by upstream solar wind and IMF conditions and provides high-latitude convection and auroral electron precipitation (including hard and soft electron precipitation) for TIEGCM. Details of the coupling between LFM and TIEGCM can be found in *Wiltberger et al.* [2004]. A causally driven model of direct entry cusp soft electron precipitation (with mean energy of several hundred eV) has recently been implemented in the CMIT model [*Zhang et al.*, 2013, 2015]. Data-model comparisons show that CMIT is capable of reproducing the variations in thermospheric density observed by satellites during quiet periods. With the implementation of soft electron precipitation, CMIT is capable of reproducing the observed density spikes during active time periods quantitatively as well.

2. Results and Discussions

The time period of the first event simulation is between 4:00 and 9:00 UT, 24 August 2005, which was also studied by *Crowley et al.* [2010]. Figure 1a shows the solar wind conditions and interplanetary magnetic fields (SW/IMFs) in the solar magnetospheric (SM) coordinates for the 24 August 2005 event. Starting from 6:10 UT, SW density and velocity increase significantly, and the IMF B_y component becomes the dominant IMF for about 3 h. Between 06:00 and 07:00 UT, the average *Kp* index is 6 and the average SW number density is above 30 cm^{-3}; therefore, intense fluxes of soft electron precipitation occur in the dayside cusp region together with intense Joule heat. Thus, both pathways of heating via soft electrons are expected in this event. The second event simulation time period is between 10:00 and 15:00 UT, 27 July 2007, and the SW/IMF conditions in the SM coordinates are shown in Figure 1b. During the whole event, the average *Kp* index is 2− and the IMF is mostly northward ($Kp = 2-$) and the Joule heating rate in the polar cusp region is much lower compared to the 24 August 2005 event. Between 13:00 and 15:00 UT, the average solar wind number density is approximately 60 cm^{-3}, which is twice as high as the first event. Therefore, intense soft electron precipitation flux in the cusp region is expected in both hemispheres, while the Joule heating rate in the cusp region is expected to be relatively small in the cusp region. Thus, the direct heating pathway is expected to be dominant in the second event. Note that since the average energy of cusp electron precipitation is proportional to the magnetosheath electron temperature, which is proportional to the SW dynamic pressure, the simulated characteristic energy

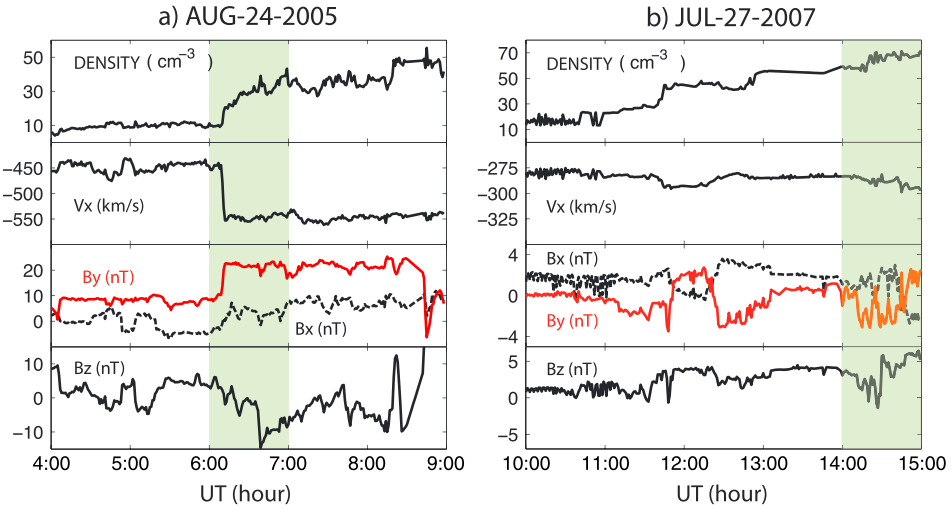

Figure 1. The SW/IMF conditions for (a) the 24 August 2005 event and (b) the 27 July 2007 event. Data are provided by J. H. King and N. Papatashvilli at ADNET, NASA GSFC, and CDAWeb.

of cusp electrons in the 24 August 2005 event is approximately twice as high as the 27 July 2007 event (276 eV versus 120 eV) [*Zhang et al.*, 2015].

Figure 2 illustrates the indirect role of soft electron precipitation in the 24 August 2005 event. Figure 2 (top left and top middle) shows the simulated distributions of Joule heating rate per unit volume ($\mathbf{J}\cdot\mathbf{E}$) in the Southern Hemisphere height integrated above 200 km altitude and averaged between 06:00 and 07:00 UT on 24 August 2005, with the cusp soft electron precipitation model switched off and switched on, respectively. Since the impacts of *F* region Joule heating are more efficient than that in the *E* region, only the height-integrated Joule heating rate between 200 and 500 km altitude is shown in Figure 2. Figure 2 (top right) shows the relative difference of thermospheric mass density at 400 km altitude between the two CMIT simulations calculated from the same time period. The location of the cusp precipitation pattern is shown using black contours in Figure 2 (top middle), together with the orbit tracks of the CHAMP satellite near 07:00 UT. The simulated peak soft electron energy flux is 4.6 mW/m^2, and the average characteristic energy between 06:00 and 07:00 UT is around 276 eV. Figure 2 (bottom) shows the simulated thermospheric mass density from the CMIT runs along CHAMP orbit together with the measured mass density of CHAMP between 04:00 and 09:00 UT. The result from a stand-alone TIEGCM simulation, which is driven by the Heelis potential model [*Heelis et al.*, 1982] with the *Hardy et al.* [1985] empirical precipitation model, is also shown in Figure 2.

Figure 2 (bottom) shows that near 7:00 UT, both CMIT simulations start to show density spikes when CHAMP traverses near the southern (7:00 UT) and northern (7:35 UT) cusp regions. The spikes are consistent with CHAMP observations, whereas both MSIS90 and stand-alone TIEGCM fail to predict the mass density spikes starting from 7:00 UT. Without soft electron precipitation, a 50% enhancement of mass density with respect to the MSIS90 density occurs in the Southern Hemisphere cusp region during the CHAMP crossing between 6:50 and 7:10 UT. The CMIT simulation without soft electron precipitation indicates that the increase in Joule heating can cause a thermospheric mass density enhancement, which is consistent with the conclusions in *Crowley et al.* [2010]. However, the magnitude of the peak enhancement is less than the observed value from CHAMP ($\approx$ 105% enhancement with respect to MSIS90). With soft electron included in the simulation, the mass density enhancement along the CHAMP orbit when crossing the southern cusp region is approximately 120% relative to MSIS90 density, and the peak density is about the same as the CHAMP observation. The controlled simulation results show that the thermospheric mass density enhancement near the southern cusp region is a consequence of the increased Joule heating rate in the *F* region mainly caused by soft electron precipitation. With the soft electron precipitation model switched on, the height-integrated Joule heating rate above 200 km near the southern cusp region averaged between 06:00 and 07:00 UT increases from 6.9 mW/m^2 to 9.7 mW/m^2 (about 40% enhancement). As shown in Figure 2, between 6:50 and 7:02 UT, the CHAMP satellite passes through the eastward edge of the simulated Southern Hemisphere cusp, and the simulated peak mass density enhancement along the CHAMP path is improved significantly and in good agreement with CHAMP when the soft electron precipitation model was switched on. Similar behaviors of Joule heating, cusp electron

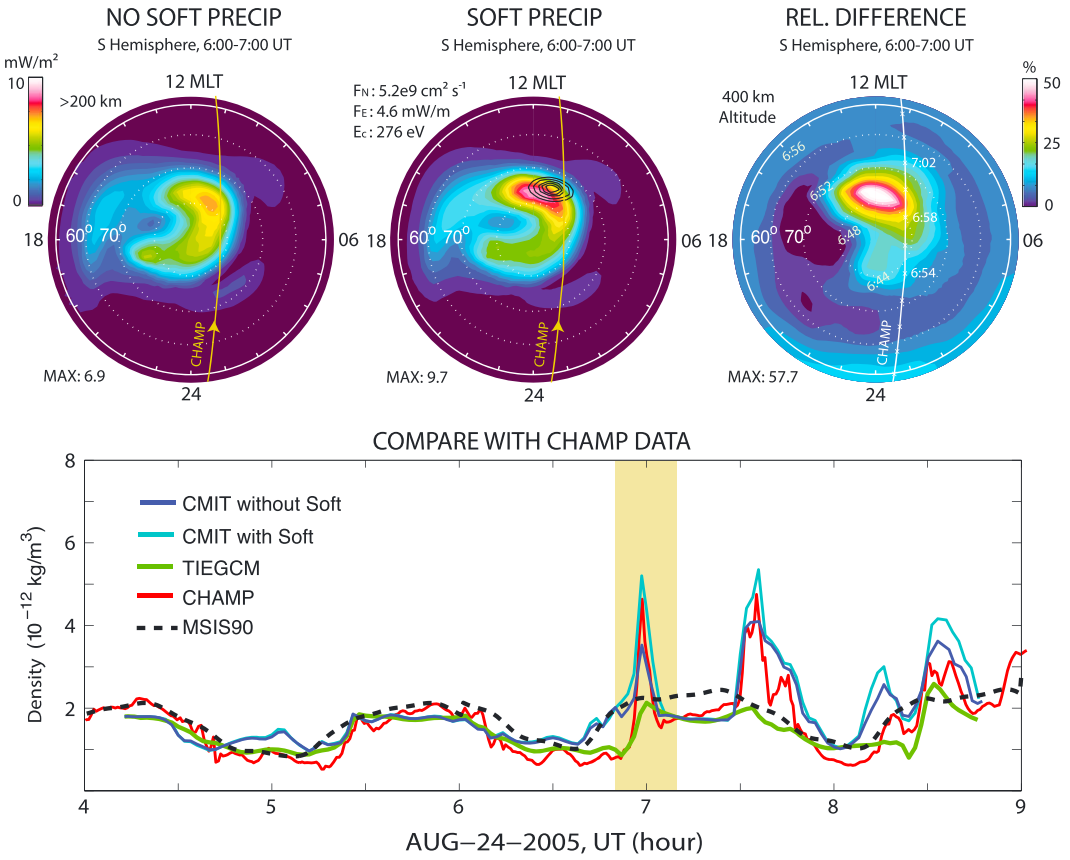

Figure 2. Distributions of average Joule heating rate in the Southern Hemisphere derived from the 24 August 2005 event simulation (top left) without soft electron precipitation, (top middle) with soft electron precipitation, and (top right) the relative enhancement of thermospheric mass density at 400 km calculated from the same time period. The time period for averaging is between 6:00 and 7:00 UT, 24 August 2005. The distribution of soft electron precipitation is shown in Figure 2 (top middle) using black contours. The CHAMP orbit around 06:50 is also shown in each panel. (bottom) Simulated thermospheric mass density along the CHAMP orbit with the soft electron precipitation model switched on (light blue) and off (dark blue), together with the densities derived from the CHAMP measurements (red), the MSIS90 empirical model (black), and the stand-alone TIEGCM simulation (green). The shaded time period indicates the CHAMP crossing of the southern polar region.

precipitation, and thermospheric mass density enhancement at 400 km altitude occur near 7:30 UT when CHAMP passes through the northern cusp region.

In the CMIT simulations, the cross polar cap potential (CPCP) derived from the MHD simulation typically is 1.5 times higher than predicted by *Weimer* [2005] empirical model [*Zhang et al.*, 2011]. Thus, in driving the TIEGCM in CMIT, we downscaled the LFM CPCP by a factor of 0.67 (1/1.5). As a consequence, the Joule heating rate in the polar cap is decreased approximately by a factor of 0.5 without soft electron precipitation. With this scaling factor, the maximum Joule heating rate between 6:30 and 7:00 is 71 mW/m^2 while the measured maximum given by DMSP is around 75 mW/m^2, as discussed in *Crowley et al.* [2010]. The scaling factor evidently more accurately represents the energy input from the magnetosphere to the ionosphere-thermosphere and is introduced in both event simulations. Without the scaling factor, the simulated mass density near the cusp region is overestimated by both CMIT simulations due to the excessive amount of Joule heat, but the relative enhancement of thermospheric density between the two controlled simulations is not determined by the scaling factor.

The direct role of soft electron precipitation in the 27 July 2007 event is shown in Figure 3. Figure 3 (top left and top middle) shows the simulated average Joule heating rate above 200 km in the Southern Hemisphere between 14:00 and 15:00 UT when the IMF B_z is mostly northward between 0 to +5 nT, with variable but small B_x and B_y. The simulated height-integrated (from 100 km to 500 km) Joule heating rate between 14:00 and 15:00 UT is around 1.5 mW/m^2 which is much less than the peak value of 71 mW/m^2 during the 24 August

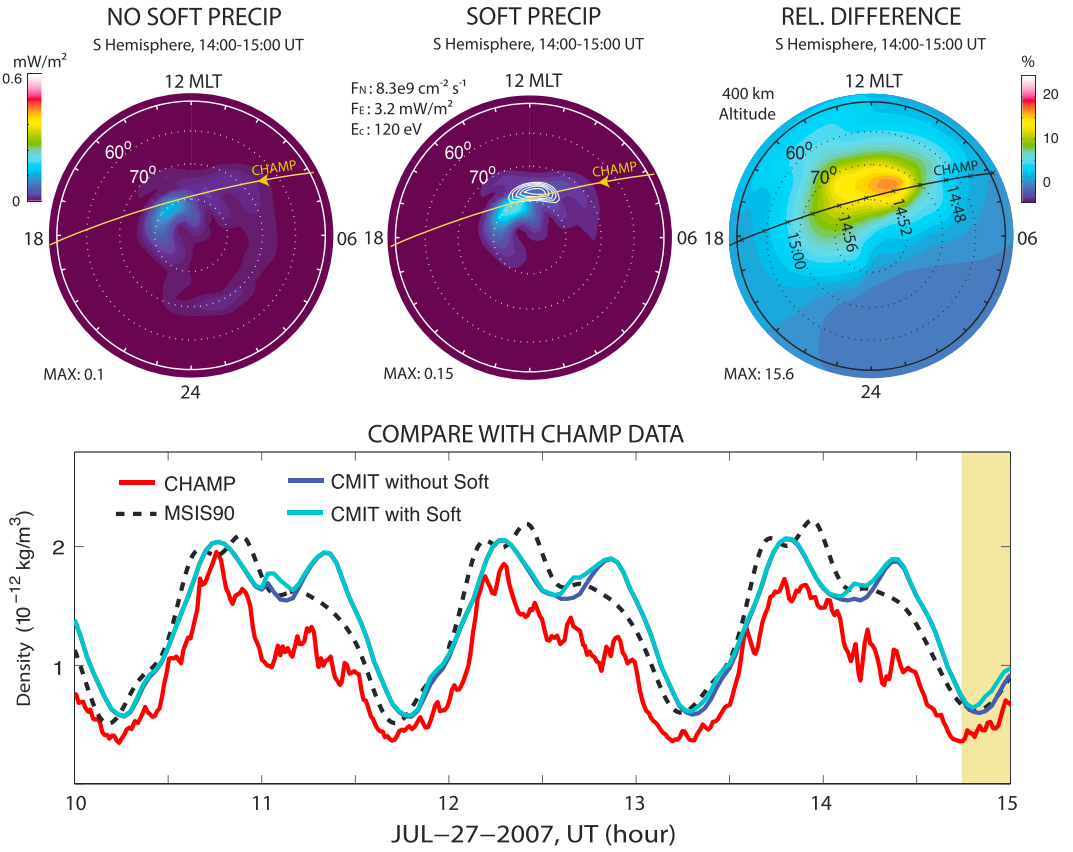

Figure 3. Distributions of average Joule heating rate in the Southern Hemisphere derived from the 27 July 2007 event simulation (top left) without soft electron precipitation, (top middle) with soft electron precipitation, and (top right) the relative enhancement of thermospheric mass density at 400 km. The average time period is between 14:00 and 15:00 UT, 27 July 2007. The distribution of soft electron precipitation is shown in Figure 3 (top middle) using white contours. The CHAMP orbits around 14:50 are shown in each panel. (bottom) Simulated thermospheric mass density along the CHAMP orbit with the soft electron precipitation model switched on (light blue) and off (dark blue), together with the densities derived from the CHAMP measurements (red), the MSIS90 empirical model (black), and the stand-alone TIEGCM simulation (green). The shaded time period indicates the CHAMP crossing of the southern polar region.

2005 event. This difference on the peak total Joule heating rate indicates that during the July 27 2007 event, the coupling between the solar wind-magnetosphere-ionosphere is much weaker in the cusp region compared to the 24 August 2005 event. In other word, the cusp Joule heating rate during the 27 July 2007 event is almost negligible. Figure 3 (top left) is derived from the CMIT simulation with the cusp soft electron precipitation model switched off, and Figure 3 (top middle) is derived from the CMIT simulation with the soft electron precipitation model switched on. The location of average cusp precipitation pattern is shown using white contours in Figure 3 (top middle), together with the orbit of the CHAMP satellite near 14:52 UT, which approximately passes through the center of the simulated cusp. Figure 3 (top right) shows the relative enhancement of thermospheric mass density due to cusp electron precipitation at 400 km altitude calculated from the same time period. Figure 3 (bottom) shows the simulated thermospheric mass density along CHAMP orbit from the two controlled simulations, together with the measured mass density between 10:00 and 15:00 UT.

Figure 3 (bottom) shows that, during the July 27 2005 event, the simulated mass density at 400 km altitude is in good agreement with predictions from the MSIS90 empirical model but slightly higher than the mass density derived from the CHAMP measurements. Between 14:00 and 15:00 UT, the simulated cusp electron precipitation in the Southern Hemisphere has a maximum energy flux around 3.2 mW/m^2 and average characteristic energy around 120 eV, which is softer than during the 24 August 2005 event. The precipitating number flux for the 27 July 2005 event has an approximately 60% higher number flux. However, the peak enhancement of thermospheric mass density at 400 km is only 15.6% relative to the background density. As shown in Figure 3 (top left and top middle), between 14:00 and 15:00 UT, the Joule heating rate above 200 km is not

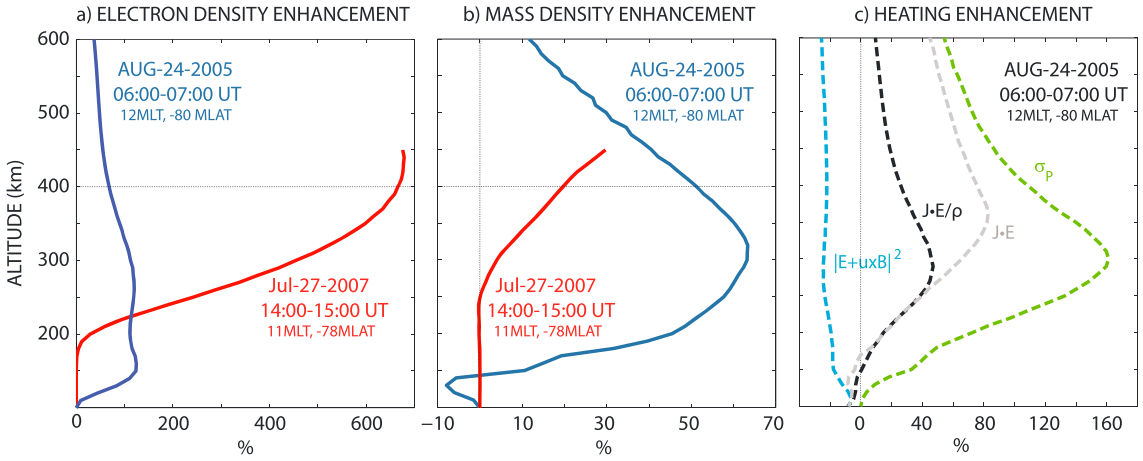

Figure 4. Height profiles of (a) electron density enhancement and (b) thermospheric mass density enhancement derived from the two event simulations when the soft electron precipitation model is switched on. For the 24 August 2005 event, the average profiles are calculated between 06:00 and 07:00 UT; for the 27 July 2007 event, the average profiles are calculated between 14:00 UT and 15:00 UT. (c) The relative height profiles of $|E + u \times B|^2$, σ_P and Joule heat (per unit mass and per unit volume) derived from the 24 August 2005 event.

significantly affected by soft electron precipitation in the cusp region. Moreover, the Joule heating rate near the cusp region is less than 0.1 mW/m^2, which indicates that the Joule heating is not the driver of thermospheric mass density in this event. Rather, the thermosphere neutrals in the southern cusp region are directly affected by the precipitating soft electrons through the energy exchange between soft electrons and ions/neutrals. As shown in Figure 3 (bottom), neither CMIT simulations nor CHAMP measurements show a significant density spike near 14:52 UT when the CHAMP satellite passes through the cusp precipitation region, which suggests that the direct heating from precipitating soft electrons is very inefficient.

Comparisons on the heating efficiency due to cusp soft electron precipitation are shown in Figure 4, which shows the altitude profiles of the relative enhancement in electron density and neutral density calculated from two fixed magnetic latitude (MLAT) and magnetic local time (MLT) locations in the cusp regions of the two events. As shown in Figure 4a, in the 24 August 2005 event, the average electron density enhancement near 300 km altitude between 06:00 and 07:00 UT is around 100%, while the enhancement in the 27 July 2007 event exceeds 600%. This difference in electron density is consistent with the fact that in the 27 July 2007 event, more cusp electrons precipitate into the ionosphere-thermosphere. The enhancement in electron density is also a consequence of enhanced electron temperature which increases the scale height of the *F* region. Figure 4b shows the relative difference of thermospheric mass density when soft electron precipitation is turned on in the two event simulations. The altitude profiles are calculated from the same fixed locations as the electron density profiles shown in the left sides of Figures 4a and 4b. Comparison shows that although the simulated electron density enhancement is approximately 6–8 times higher in the 27 July 2007 event, the thermospheric mass density enhancement is much less than that in the 24 August 2005 event, especially below 300 km altitude. Note that in the 24 August 2005 event, when cusp soft electron precipitation is switched on, a relative decrease of thermospheric mass density of approximately 8% occurs below 150 km altitude. As shown in Figure 4c, this depletion of mass density in the 24 August 2005 event at low altitude is caused by the self-consistent, nonlinear interaction between the magnetosphere and the ionosphere-thermosphere system since the local electric field is dynamically determined by the coupling between the magnetosphere and ionosphere-thermosphere which is affected by the cusp electron precipitation. When soft electron precipitation is included, the *F* region Pedersen conductivity σ_P in the cusp region increases, which results in a decrease in the local electric field $|\mathbf{E} + \mathbf{u} \times \mathbf{B}|$. The Joule heating rate per unit mass ($\sigma_P |\mathbf{E} + \mathbf{u} \times \mathbf{B}|^2 / \rho$) increases up to 40% near 300 km altitude but decreases about 10% below 150 km altitude.

Additional numerical experiments have also been done to isolate the efficiencies of the direct and indirect pathways of thermospheric heating when soft electron precipitation and Joule heating are colocated in the cusp region. In the direct heating experiment, the precipitating soft electron fluxes are only used in the

electron temperature equation. By doing this, the soft electrons are only allowed to directly exchange energy with ionospheric plasmas and thermospheric neutrals. As a consequence, the electron density and ionization profile in the cusp region are not expected to be directly affected by the precipitation soft electrons. Of course, the direct heating test simulation is not physical; however, by doing this, the *F* region Pedersen conductivity is not significantly affected by the soft electrons; therefore, the effect of the indirect heating pathway is approximately excluded from the test simulation. In the indirect heating experiment, the precipitating soft electrons are only allowed to modify the ionization profiles used in the ion continuity equations, and the direct heating term in the electron temperature equation associated with soft electron precipitation is turned off. The indirect heating simulation is also not physical, but it allows the model to approximately exclude the direct energy exchange from soft electrons to ionospheric plasma and thermospheric neutrals, which is used to quantify the efficiency of the indirect heating pathway. The test simulations are driven by southward IMF conditions ($N_{SW} = 25\text{cm}^{-3}$, $v_{SW} = 400$ km/s, $B_z = -5$ nT, and $F_{10.7} = 150$), and the results described below are averaged from the first simulation hour. Compared to a baseline CMIT simulation without soft electron precipitation, in the direct heating experiment, the direct energy exchange between precipitating soft electrons and ions/neutrals only causes up to 10% enhancement of thermospheric mass density at 400 km altitude, while in the indirect heating experiment, the increased *F* region Joule heating rate causes up to 60% enhancement of thermospheric mass density at 400 km altitude. Note that the 10% enhancement in the direct heating simulation may be overestimated due to the underestimation of ion cooling since the ionization effect of soft electron precipitation is neglected in the simulation. A self-consistent CMIT simulation with both indirect and direct heating pathways enabled has approximately 80% enhancement of mass density at 400 km, which suggests the effects of nonlinear interaction between the two heating pathways. The effects of soft electron precipitation on thermospheric mass density enhancements derived from the direct and indirect pathway simulations are consistent with the simulation results from *Deng et al.* [2013]. These nonphysical test simulation results suggest that during moderate southward IMF driving conditions, the direct pathway of thermospheric heating via cusp soft electron precipitation is much less efficient than the indirect pathway, which is possibly a consequence of low efficiency in direct momentum and energy exchange from both elastic and inelastic collisions between the neutrals and electrons. Since elastic electron-neutral collisions are extremely inefficient due to the large neutral-electron mass ratio effect, the dominant processes of electron-neutral cooling are actually inelastic collisions. The most important inelastic collision processes are the excitations of N_2 vibrational/rotational states, O_2 vibrational/rotational states, O(3S) electronic fine structure, and O(1D). These inelastic collision processes are also very inefficient at moving energy from the electrons to the neutrals.

Note that in the hydrostatic description of the ionosphere-thermosphere used in the CMIT model, the *F* region thermospheric mass density perturbations are dominated by the heating effects associated with precipitation soft electrons which affects the neutral temperature. However, other processes such as nonhydrostatic effects, changes in the neutral wind, and composition may also be important in the enhancement of *F* region thermospheric mass density [e.g., *Deng et al.*, 2008, 2013; *Liu et al.*, 2014]. Therefore, further studies are needed to investigate the pathways of *F* region thermospheric mass density enhancements besides the heating effects.

3. Summary

We use the coupled magnetosphere-ionosphere-thermosphere (CMIT) model to investigate the roles of soft electron precipitation on the *F* region thermospheric heating and to investigate the relationship between the Joule heating and soft electron precipitation as large-scale drivers for thermospheric mass density enhancement in the cusp region. The 24 August 2005 event simulations suggest that when the Joule heating rate is large in the cusp region, soft electron precipitation plays a crucial role in producing the *F* region thermospheric mass density enhancement through an indirect heating pathway, that is, by increasing the Joule heating rate above 200 km. On the other hand, the 27 July 2007 event simulation demonstrates that when the Joule heating rate is small in the cusp region, the efficiency of the direct heating associated with precipitating soft electrons on *F* region thermospheric mass density is relatively low. The self-consistent electric field generally decreases locally in response to additional conductivity introduced by soft electron precipitation. The relative magnitudes of the decrease in the electric field strength and the increase in conductivity are such that the Joule heating rate increases above 200 km but can slightly decrease at lower altitudes.

Acknowledgments
The research was supported by NASA grants NNX11AO59G and NNX11AJ10G and AFOSR grant 14RT0299. Computing resources were provided by National Center for Atmospheric research (NCAR) under CISL projects 3761009 and UDRT0001. NCAR is sponsored by the NSF. The SW/IMF data sets are provided by J.H. King and N. Papatashvilli at ADNET, NASA GSFC, and CDAWeb. The CHAMP data sets are provided by Eric Sutton. Simulation data are available from B. Zhang (bzhang@dartmouth.edu).

Michael Liemohn thanks Jianpeng Guo and one anonymous reviewer for their assistance in evaluating this paper.

References

Carlson, H. C., T. Spain, A. Aruliah, A. Skjaeveland, and J. Moen (2012), First-principles physics of cusp/polar cap thermospheric disturbances, *Geophys. Res. Lett.*, *39*, L19103, doi:10.1029/2012GL053034.

Crowley, G., D. J. Knipp, K. A. Drake, J. Lei, E. Sutton, and H. Lühr (2010), Thermospheric density enhancements in the dayside cusp region during strong B_Y conditions, *Geophys. Res. Lett.*, *37*, L07110, doi:10.1029/2009GL042143.

Demars, H. G., and R. W. Schunk (2007), Thermospheric response to ion heating in the dayside cusp, *J. Atmos. Sol. Terr. Phys.*, *69*, 649–660, doi:10.1016/j.jastp.2006.11.002.

Deng, Y., A. D. Richmond, A. J. Ridley, and H.-L. Liu (2008), Assessment of the non-hydrostatic effect on the upper atmosphere using a general circulation model (GCM), *Geophys. Res. Lett.*, *35*, L01104, doi:10.1029/2007GL032182.

Deng, Y., T. J. Fuller-Rowell, R. Akmaev, and A. J. Ridley (2011), Impact of the altitudinal Joule heating distribution on the thermosphere, *J. Geophys. Res.*, *116*, A05313, doi:10.1029/2010JA016019.

Deng, Y., T. J. Fuller-Rowell, A. J. Ridley, D. Knipp, and R. E. Lopez (2013), Theoretical study: Influence of different energy sources on the cusp neutral density enhancement, *J. Geophys. Res. Space Physics*, *118*, 2340–2349, doi:10.1002/jgra.50197.

Hardy, D. A., M. S. Gussenhoven, A. F. Geophysics, A. F. Base, and E. Holeman (1985), A statistical model of auroral electron precipitation, *J. Geophys. Res.*, *90*, 4229–4248.

Heelis, R. A., J. K. Lowell, and R. W. Spiro (1982), A model of the high-latitude ionosphere convection pattern, *J. Geophys. Res.*, *87*, 6339–6345.

Huang, Y., A. D. Richmond, Y. Deng, and R. Roble (2012), Height distribution of Joule heating and its influence on the thermosphere, *J. Geophys. Res.*, *117*, A08334, doi:10.1029/2012JA017885.

Knipp, D., et al. (2011), Extreme Poynting flux in the dayside thermosphere: Examples and statistics, *Geophys. Res. Lett.*, *38*, L16102, doi:10.1029/2011GL048302.

Liu, H., H. Lühr, V. Henize, and W. Köhler (2005), Global distribution of the thermospheric total mass density derived from CHAMP, *J. Geophys. Res.*, *110*, A04301, doi:10.1029/2004JA010741.

Liu, R., H. Lühr, and S.-Y. Ma (2010), Storm-time related mass density anomalies in the polar cap as observed by CHAMP, *Ann. Geophys.*, *28*, 165–180, doi:10.5194/angeo-28-165-2010.

Liu, X., J. P. Thayer, A. Burns, W. Wang, and E. Sutton (2014), Altitude variations in the thermosphere mass density response to geomagnetic activity during the recent solar minimum, *J. Geophys. Res. Space Physics*, *119*, 2160–2177, doi:10.1002/2013JA019453.

Lühr, H. (2004), Thermospheric up-welling in the cusp region: Evidence from CHAMP observations, *Geophys. Res. Lett.*, *31*, L06805, doi:10.1029/2003GL019314.

Lyon, J., J. Fedder, and C. Mobarry (2004), The Lyon-Fedder-Mobarry (LFM) global MHD magnetospheric simulation code, *J. Atmos. Sol. Terr. Phys.*, *66*(15–16), 1333–1350, doi:10.1016/j.jastp.2004.03.020.

Merkin, V. G., and J. G. Lyon (2010), Effects of the low-latitude ionospheric boundary condition on the global magnetosphere, *J. Geophys. Res.*, *115*, A10202, doi:10.1029/2010JA015461.

Mishin, E., E. Sutton, G. Milikh, I. Galkin, C. Roth, and M. Förster (2012), F2-region atmospheric gravity waves due to high-power HF heating and subauroral polarization streams, *Geophys. Res. Lett.*, *39*, L11101, doi:10.1029/2012GL052004.

Rentz, S. (2009), The upper atmospheric fountain effect in the polar cusp region, PhD thesis, Deutsches GeoForschungsZentrum GFZ, Potsdam, doi:10.2312/GFZ.b103-09050.

Rentz, S., and H. Lühr (2008), Climatology of the cusp-related thermospheric mass density anomaly, as derived from CHAMP observations, *Ann. Geophys.*, *26*, 2807–2823.

Richmond, A. D. (1992), Assimilative mapping of ionospheric electrodynamics, *Adv. Space Res.*, *12*(6), 59–68, doi:10.1016/0273-1177(92)90040-5.

Roble, R. G., E. C. Ridley, and A. D. Richmond (1988), A coupled thermosphere/ionosphere general circulation model, *Geophys. Res. Lett.*, *15*(88), 1325–1328, doi:10.1029/GL015i012p01325.

Roble, R. G., and E. C. Ridley (1994), A thermosphere-ionosphere-mesosphere-electrodynamics general circulation model (TIME-GCM): Equinox solar cycle minimum simulations (300–500 km), *Geophys. Res. Lett.*, *21*, 417–420, doi:10.1029/93GL03391.

Wang, W., M. Wiltberger, A. G. Burns, S. C. Solomon, T. L. Killeen, N. Maruyama, and J. G. Lyon (2004), Initial results from the coupled magnetosphere-ionosphere-thermosphere model: Thermosphere-ionosphere responses, *J. Atmos. Sol. Terr. Phys.*, *66*(15–16), 1425–1441, doi:10.1016/j.jastp.2004.04.008.

Wang, H., H. Lühr, K. Husler, and P. Ritter (2011), Effect of subauroral polarization streams on the thermosphere: A statistical study, *J. Geophys. Res.*, *116*, A03312, doi:10.1029/2010JA016236.

Weimer, D. R. (2005), Improved ionospheric electrodynamic models and application to calculating Joule heating rates, *J. Geophys. Res.*, *110*, A05306, doi:10.1029/2004JA010884.

Wiltberger, M., W. Wang, A. G. Burns, S. Solomon, J. Lyon, and C. Goodrich (2004), Initial results from the coupled magnetosphere ionosphere thermosphere model: Magnetospheric and ionospheric responses, *J. Atmos. Sol. Terr. Phys.*, *66*(15–16), 1411–1423, doi:10.1016/j.jastp.2004.03.026.

Zhang, B., W. Lotko, M. J. Wiltberger, O. J. Brambles, and P. A. Damiano (2011), A statistical study of magnetosphere-ionosphere coupling in the Lyon-Fedder-Mobarry global MHD model, *J. Atmos. Sol. Terr. Phys.*, *73*, 686–702, doi:10.1016/j.jastp.2010.09.027.

Zhang, B., W. Lotko, O. Brambles, M. Wiltberger, W. Wang, P. Schmitt, and J. Lyon (2012), Enhancement of thermospheric mass density by soft electron precipitation, *Geophys. Res. Lett.*, *39*, L20102, doi:10.1029/2012GL053519.

Zhang, B., O. Brambles, W. Lotko, W. Dunlap-Shohl, R. Smith, M. Wiltberger, and J. Lyon (2013), Predicting the location of polar cusp in the Lyon-Fedder-Mobarry global magnetosphere simulation, *J. Geophys. Res. Space Physics*, *118*, 6327–6337, doi:10.1002/jgra.50565.

Zhang, B., W. Lotko, O. Brambles, M. Wiltberger, W. Wang, and J. Lyon (2015), Electron precipitation models in global magnetosphere simulations, *J. Geophys. Res. Space Physics*, *120*, 1035–1056, doi:10.1002/2014JA020615.